RSC Advances

PAPER

View Article Online
View Journal | View Issue

Cite this: *RSC Adv.*, 2024, **14**, 32554

Pressure induced emission enhancement (PIEE) in solid-state 2,3,4,5-tetraphenylthiophene: a QM/MM study†

Yarong Gu *

Organic fluorophores exhibit pressure-dependent behaviors that are often irregular and contingent upon the specific system. Elucidating how pressure influences these behaviors is essential for the accurate design of piezochromic materials. Here, we conducted an exhaustive theoretical analysis of the excited-state decay processes of crystalline 2,3,4,5-tetraphenylthiophene (TPT) at high pressure through a combined quantum mechanics and molecular mechanics (QM/MM) method. The study revealed that the fluorescence quantum yield experiences a pronounced initial increase owing to the decrease of nonradiative decay IC rate (k_{IC}). The suppression of low-frequency modes results in the decrease of λ_e, and then reduces the electron-vibration couplings, and finally slows down the non-radiative process. Our research provides detailed mechanism analyses on PIEE properties of solid state TPT, aiding the rational design of advanced PIEE materials.

Received 4th September 2024
Accepted 9th October 2024

DOI: 10.1039/d4ra06387b

rsc.li/rsc-advances

Introduction

Stimuli-responsive luminescent materials have garnered significant attention due to their practical applications in optical devices and sensors.[1–4] High-pressure technology has been extensively utilized for probing the photophysical properties of organic luminescent compounds. It has been generally observed that the luminescence of organic luminophores in the condensed phase is diminished by pressurization as intermolecular interactions intensify. Therefore, the phenomenon of pressure-induced emission enhancement (PIEE) observed in some organic luminophores is particularly intriguing.

The PIEE phenomenon is quite astonishing. It has been suggested that the suppression of intramolecular motion could be the reason behind the PIEE effect.[5–7] Additionally, it is hypothesized that a change in molecular conformation due to pressure is what leads to the increased luminescence.[8,9] However, the intricate relationship between structure and properties in PIEE remains obscure, primarily because of the limited availability of structural and photophysical characterization methods suitable for high-pressure studies. To harness the improved efficiency of PIEE and create more effective solid-state light emitters, there is an urgent need for a thorough and exhaustive investigation into the underlying mechanisms.

The dynamics of the excited states in organic molecular clusters are fundamental to comprehending the photophysical of organic light-emitting solids. Optical spectra resolved by vibration and the decay rate constants of the excited states are effective characterizations for investigating the luminescent mechanism. A theoretical study of the PIEE mechanism can uncover structural and excited-state dynamics at various pressure levels. In experiments, the hydrostatic pressure applied to the sample is uniform. Thus, computationally, the hydrostatic compression process can be simplified by considering the volume reduction of the crystal lattice. From this perspective, dispersion-corrected density functional theory (DFT-D) on a plane-wave basis provides an efficient approach to simulate the crystal structure under a specific external pressure. Building on this, Shuai's group explore the excited-state dynamics of molecular clusters in organic crystals through the formalism of the thermal vibration correlation function, integrated with hybrid quantum mechanics/molecular mechanics (QM/MM) simulations.[10–12]

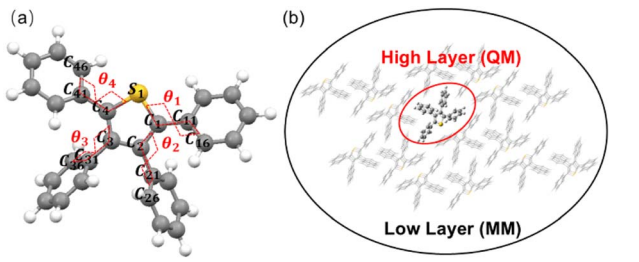

Fig. 1 (a) Chemical structures and optimised 'ball-stick' structures of TPT. The interesting dihedral angles (θ_1, θ_2, θ_3, θ_4) are marked. (b) ONIOM model in the solid state: the central molecule (48 atoms) is treated as high layer and the surrounding molecules (2352 atoms) are chosen low layer.

Department of Electronics, Xinzhou Normal University, Xinzhou, 034000, People's Republic of China. E-mail: guyr1990@163.com

† Electronic supplementary information (ESI) available. See DOI: https://doi.org/10.1039/d4ra06387b

In this research, we explore the impact of pressurization on the photophysical characteristics of 2,3,4,5-tetraphenylthiophene (TPT) (Fig. 1a). Our objective is to clarify the precise influence of pressure in dynamics of the excited states for solid-state TPT.

Computational methods

The initial single-crystal structures of TPT at different hydrostatic pressures originate from experimental high-resolution X-ray diffraction (ADXRD) data. The experimental XRD patterns were refined by using the reflex module combined in the Materials Studio Software.[13] The 'powder refinement' tool was used to setup the parameter of refinement. Convergence quality is fine. Geometries of TPT in the ground (S_0) and first singlet excited (S_1) states were obtained by using DFT and TDDFT with B3LYP functional respectively.[14–16] Based on the crystal structures obtained from DFT-D calculations,[17] we set up the QM/MM models for each TPT crystal at both ambient and high pressures (Fig. 1b). The QM/MM model was built by cutting a cluster from the crystal of size 2 × 3 × 2. The central molecule (48 atoms) was treated as the QM region and others were all MM molecules (2352 atoms). During the QM/MM simulations, geometry optimizations were performed on the QM molecule with the MM molecules frozen. The universal force field (UFF) was used to describe the molecular force field. While the electronic embedding was applied to describe the coupling of the QM/MM interface.[18] In the model, the QM region and MM region interact *via* electronic embedding. The partial charges from the MM region are included in the QM Hamiltonian, which provides a more accurate description of the electrostatic interaction and, in addition, allows the wave function to respond to the charge distribution of the MM region. All the above calculations were performed in the Gaussian 16 package.[19] The fluorescence rate (k_r) is calculated using Einstein's spontaneous emission equation[20–22] as follows, $k_r = \frac{8\pi^2 \nu_{fi}^3}{3\varepsilon_0 \hbar c^3} \mu_{fi}^2 \approx \frac{f \nu_{fi}^3}{1.499}$, Where μ_{fi} is the electric transition dipole moment between the initial and the final electronic states, f is the oscillator strength and ν_{fi} is the vertical energy in units of wave numbers (cm^{-1}). The nonradiative decay IC rate (k_{ic})is the nonradiative internal rate, which was deduced based on Fermi's golden rule and the first-order perturbation theory, and it can be written as follows, $k_{ic} = \sum_{kl} \frac{1}{\hbar^2} R_{kl} \int_{-\infty}^{\infty} dt \left[e^{i\omega_{if} t} Z_i^{-1} \rho_{ic}(t,T) \right]$, where $R_{kl} = \langle \phi_f | P_{fk} | \phi_i \rangle \langle \phi_i | P_{fi} | \phi_f \rangle$ is the nonadiabatic electronic coupling, Z_i is the partition function, $\rho_{ic}(t,T) = \mathrm{Tr}(\hat{P}_{fk} e^{i\tau_f \hat{H}_f} \hat{P}_{fi} e^{i\tau_i \hat{H}_i})$ and is the thermal vibration correlation function (TVCF).[23,24] k_r and k_{ic} were calculated using the MOMAP (Molecular Materials Property Prediction Package) program.[11,25,26]

Results and discussion

It is widely acknowledged that the molecule geometry determines its electronic structure and then affects its luminescent properties. Based on the initial crystal packing, we do the optimization of molecules geometry in the ground state (S_0) and the excited states (S_1) in the solid phase. The selected vital dihedral angles (Fig. 1a) for different states of TPT are collected in Tables S1 and S2.† When compressed, the changes of torsion angle θ_1 and θ_3 in S_0 state are minimal. However, the θ_2 increases and the θ_4 decreases remarkably. The same trend is shown in S_1 state. Our calculation results show that the changes in dihedral angles θ_2 and θ_4 dominate the structural change, and then has effect on the optical property. Increasing hydrostatic pressures are structural modifications occurring in the crystal structures. It means that how changing intermolecular distance in crystal packing. Also explain the intermolecular distance make any significance in the emission property.

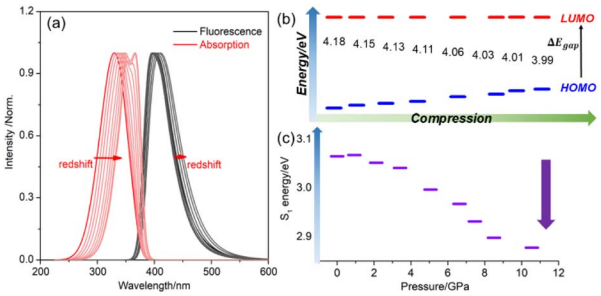

Fig. 2 Calculated vibrationally resolved normalized (a) absorption and emission spectra for TPT crystal at different pressures. (b) The change of HOMO–LUMO energy gaps (ΔE_{gap}) with increasing pressure. (c) The change of energy level of S_1.

The vibrationally resolved absorption and emission spectra calculated at varying pressures are depicted in Fig. 2a. A significant redshift is noticeable in the absorption bands of TPT under compression as the pressure rises from ambient to 8.5 GPa. Fig. 2b exhibits the changes of the highest occupied molecular orbital (HOMO) and the lowest unoccupied molecular orbital (LUMO) with increasing pressure. HOMO energy level raises, thus leading to the decreases of HOMO–LUMO energy gaps (ΔE_{gap}) from 4.18 eV to 3.99 eV (Table S3†). The reduced HOMO–LUMO energy gaps would be responsible for the redshift in absorption upon compression. At the same time, the emission spectra also exhibit redshift phenomenon, which are ascribable to the decrease of S_1 energy level (Fig. 2c and listed in Table S3†). The calculated singlet–triplet (S_1 and T_1) energy gap is 1.19 eV, which is so high that the intersystem crossing process from S_1 to T_1 could be neglected. The similar approach had been mentioned in hexaphenylsilole.[7] Therefore, the internal conversion (IC) process from S_1 to S_0 is regarded as the main non-radiative decay pathway in their solid state.

The calculated k_r, k_{ic} and Φ_F (which represents fluorescent efficiency $\Phi_F = \frac{k_r}{k_{r+k_{ic}}}$) are shown in Fig. 3a and listed in Table S4.† k_r decreases from 2.384×10^8 s^{-1} at 0 GPa to a minimum of 2.100×10^8 s^{-1} at 8.50 GPa. There is a slight increase from 2.348×10^8 s^{-1} at 0.93 GPa to 2.386×10^8 s^{-1} at 3.41 GPa, followed by a gradual decrease. While k_{ic} decreases from 5.803 $\times 10^8$ s^{-1} at 0 GPa to 2.060×10^8 s^{-1} at 2.12 GPa, then increases

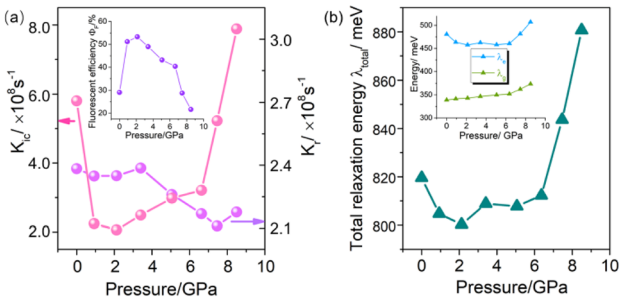

Fig. 3 (a) The calculated k_r, k_{ic} and Φ_F. (b) Reorganization energies $\lambda_{g(e)}$ and total reorganization energies λ_{total} of TPT in solid state at different pressures.

to $2.488 \times 10^8\ s^{-1}$ at 3.41 GPa, and continues to rise sharply to $7.884 \times 10^8\ s^{-1}$ at 8.50 GPa. Φ_F exhibits an obvious increase to 53.29% when the pressure increases to 2.12 GPa, followed by a gradual decrease.

To gain a deeper understanding of the complex optical phenomena, the main factors affecting k_r and k_{ic} are analyzed. According to the Einstein spontaneous emission relationship $k_r = \frac{f\nu_{fi}^2}{1.499}$, k_r is proportional to the adiabatic excitation energy (ν_{fi}) and the oscillator strength (f). From Table S5,† f and ν_{fi} keeps weak change at 0–8.50 GPa. So the change of k_r is small at this range. Compared with the change of k_r, k_{ic} exhibits an obvious change at the whole compression progress. Therefore, the change of Φ_F mainly results from k_{ic}. According to the approximate form of k_{ic}, the adiabatic excitation energy (ν_{fi}) and the reorganization energy (λ) are two important factors to determine the k_{ic}. Reorganization energy λ, which demonstrates the vibrations' ability to accept the excited-state electronic energy, can be expressed in the harmonic oscillator approximation: $\lambda = \sum_k \hbar\omega_k HR_k$ and $HR_k = \frac{\omega_k D_k^2}{2\hbar}$. HR_k is the Huang–Rhys factor for the kth mode and D_k represents the displacement along the kth normal mode between S_0 and S_1 electronic states. The total relaxation energy with the summation of all normal modes is λ_g and λ_e. When considering the difference between the potential energy surfaces in the ground and excited states, there are two sets of reorganization energy, $\lambda_{k,g}$ and $\lambda_{k,e}$. The total reorganization energy with the summation of all normal modes is λ_g and λ_e.

As can be seen from Fig. 3b, λ_{total} decreases with pressure at 0–2.12 GPa. When the pressure is beyond 2.12 GPa, λ_{total} steadily increases. Moreover, the change of ν_{fi} is weak during the whole compression process (Table S5†). Thus, the change of k_{ic} would be attributed to λ_{total}. Decreasing of λ_{total} indicates that molecular packing limits the vibrational recombination within the molecule, thereby reducing k_{ic}. At 0–2.12 GPa, the decrease of λ_{total} mainly depends on the decrease of λ_e. At 3.41–8.50 GPa, the increase of λ_{total} mainly depends on λ_e and λ_g. Fig. 4 shows the $\lambda_{k,e}$ *versus* ω_k at different pressures. We find that the contribution of low-frequency (LF, <500 cm^{-1}) modes to the total λ_e gradually increased from 50% to 52% in the lower pressure range of 0–2.12 GPa (Table S6†), while the contribution

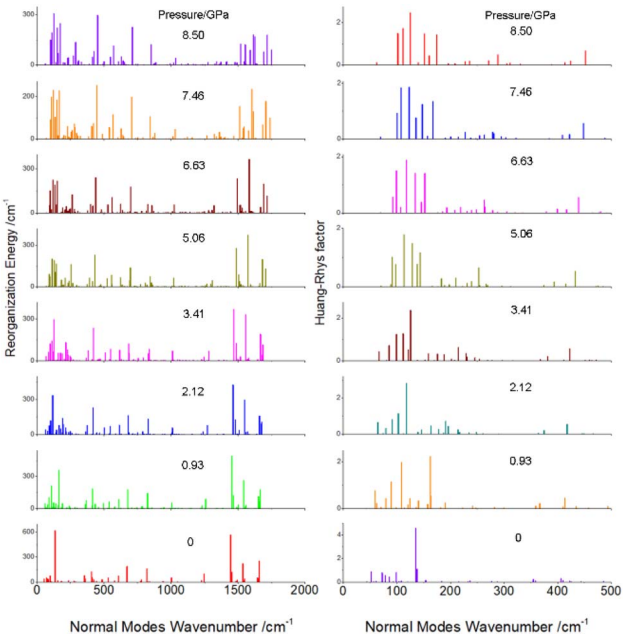

Fig. 4 Calculated Huang–Rhys factor HR_k (right) and reorganization energies $\lambda_{k,e}$ (left) *versus* the normal mode frequencies for TPT molecules in solid state at different pressure.

of high-frequency (HF, 1400–1800 cm^{-1}) modes decreases from 50% to 48% in this pressure range. HR_k *versus* ω_k are also shown in Fig. 4, which characterizes the vibrational quanta emitted in the excited-state relaxation process. It is obviously that the HR_k of low-frequency modes are remarkably reduced with increasing pressure at 0–2.12 GPa. Therefore, the decrease in λ_e in pressure range of 0–2.12 GPa mainly comes from the reduced HR_k of the low-frequency modes. When the pressure is between 3.41 and 8.50, the enhanced HR_k of the low-frequency modes would result in the increase of $\lambda_{e(g)}$ (Fig. S1 and S2).† Moreover, at 0 GPa, the large HR factors 4.6 (135 cm^{-1}) corresponds to the torsional motions (shown as Fig. S1† insets) of tetraphenyl and central thiophene in low frequency regions (<500 cm^{-1}). The HR factors at 2.12 GPa decreases with the large factors being 2.8

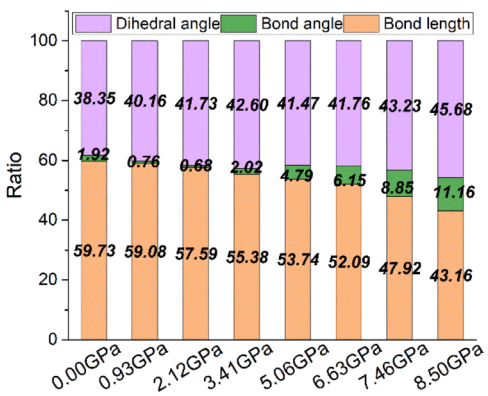

Fig. 5 Contributions of the reorganization energy λ_e from bond lengths (organ), bond angles (green) and dihedral angles (purple) for TPT in solid state.

(118 cm^{-1}). The calculation results indicate that the rotational motions in low frequency regions (<500 cm^{-1}) are suppressed under high pressure. Therefore, the non-radiative energy consumption way *via* torsional motions is hinder by the restricted intramolecular rotation effect, and then promote fluorescent efficiency in the pressure range of 0–2.12 GPa.[7,8,27]

Furthermore, to explore the effect of molecular geometry on the reorganization energies, the contributions from bond lengths, bond angles and dihedral angles are calculated, corresponding results are shown in Fig. 5 and Table S7.† When the pressure is below 2.12 GPa, the contribution of dihedral angle increases from 38.35% to 41.73%, while them of bond angle and bond length reduce to 0.68% and 57.59%, respectively. Thus, it is further proved the effect of phenyl rotor rotation on the non-radiative transition.

Conclusions

In this work, we systematically study the photophysical properties of solid state TPT using QM/MM methods. Energy gap, HR factors, reorganisation energy, excited-state dynamics as well as fluorescence efficiency are all calculated and analysed based on the first-principles methods. The results indicate that the absorption band experiences remarkable red-shift, which is ascribe to the reduced HOMO–LUMO energy gaps at the S_0 equilibrium geometries upon compression. Emission shifts are minor with increasing pressure up to 8.50 GPa, which result from the decrease of S_1 energy level. The non-radiative rate constants gradually decrease upon compression at 0–2.12 GPa and then increase with increasing pressure up to 8.50 GPa. In accordance with the excited-state decay rate constants, the fluorescence quantum efficiency undergoes a fast growth from 29.11% (0 GPa) to 53.29% (2.12 GPa) and then reduce from there on. The calculated reorganisation energy and HR factors result indicate that the suppression of low-frequency modes results in the decrease of λ_e, and then reduces the electron-vibration couplings, finally slows down the non-radiative process. The non-radiative process retards, on the contrary radiative process strengthen. The work not only offers an in-depth examination of the PIEE characteristics in solid TPT, but also a typical example for using QM/MM model to simulate molecular environment in solid state.

Data availability

The data supporting this article have been included as part of the ESI.†

Conflicts of interest

There are no conflicts to declare.

Acknowledgements

This work was supported by the National Science Foundation of China (NSFC) (12304266), the Applied Basic Research program of Shanxi Province (202103021223361). The authors thank HZWTECH for providing technical exchange support for the MOMAP program and acknowledge HZWTECH for providing computation facilities.

Notes and references

1 C. Zhao, Z. Ding, Y. Zhang, Z. Ni, S. Li, S. Gong, B. Zou, K. Wang and L. Yu, *Chem. Sci.*, 2023, **14**, 1089–1096.
2 P. Zuo, Y. Qu, Q. Zheng, L. Liao and Z. Jiang, *Mater. Chem. Front.*, 2023, **7**, 1760–1780.
3 S. Yang, Z. Feng, Z. Fu, K. Zhang, S. Chen, Y. Yu, B. Zou, K. Wang, L. Liao and Z. Jiang, *Angew Chem. Int. Ed. Engl.*, 2022, **61**, e202206861.
4 Z. Ma, Q. Li, J. Luo, S. Li, L. Sui, D. Zhao, K. Yuan, G. Xiao, J. Tang, Z. Quan and B. Zou, *J. Am. Chem. Soc.*, 2021, **143**, 15176–15184.
5 Y. Gu, K. Wang, Y. Dai, G. Xiao, Y. Ma, Y. Qiao and B. Zou, *J. Phys. Chem. Lett.*, 2017, **8**, 4191–4196.
6 Y. Gu, H. Liu, R. Qiu, Z. Liu, C. Wang, T. Katsura, H. Zhang, M. Wu, M. Yao, H. Zheng, K. Li, Y. Wang, K. Wang, B. Yang, Y. Ma and B. Zou, *J. Phys. Chem. Lett.*, 2019, **10**, 5557–5562.
7 T. Zhang, W. Shi, D. Wang, S. Zhuo, Q. Peng and Z. Shuai, *J. Mater. Chem. C*, 2019, **7**, 1388–1398.
8 J. Zhao, Y. Zeng and X. Zheng, *Chem. Mater.*, 2022, **34**, 10711–10720.
9 J. Yang, J. Qin, P. Geng, J. Wang, M. Fang and Z. Li, *Angew Chem. Int. Ed. Engl.*, 2018, **57**, 14174–14178.
10 Z. Shuai and Q. Peng, *Phys. Rep.*, 2014, **537**, 123–156.
11 Z. Shuai, *Chin. J. Chem.*, 2020, **38**, 1223–1232.
12 Z. Shuai and Q. Peng, *Natl. Sci. Rev.*, 2017, **4**, 224–239.
13 G. E. Engel, S. Wilke, K. D. M. Harris and F. J. J. Leusen, *Appl. Cryst.*, 1999, **32**, 1169.
14 R. G. Parr, *Annu. Rev. Phys. Chem.*, 1983, **34**, 631–656.
15 A. J. Cohen, P. Mori-Sanchez and W. Yang, *Chem. Rev.*, 2012, **112**, 289–320.
16 K. Burke, J. Werschnik and E. K. Gross, *J. Chem. Phys.*, 2005, **123**, 62206.
17 E. Runge and E. Gross, *Phys. Rev. Lett.*, 1984, **52**, 997–1000.
18 T. Vreven, K. S. Byun, I. Komáromi, S. Dapprich, J. A. Montgomery Jr, K. Morokuma and M. J. Frisch, *J. Chem. Theory Comput.*, 2006, **2**, 815–826.
19 M. J. Frisch, G. W. Trucks, H. B. Schlegel, G. E. Scuseria, M. A. Robb, J. R. Cheeseman, G. Scalmani, V. Barone, G. A. Petersson, H. Nakatsuji, X. Li, M. Caricato, A. V. Marenich, J. Bloino, B. G. Janesko, R. Gomperts, B. Mennucci, H. P. Hratchian, J. V. Ortiz, A. F. Izmaylov, J. L. Sonnenberg, D. Williams-Young, F. Ding, F. Lipparini, F. Egidi, J. Goings, B. Peng, A. Petrone, T. Henderson, D. Ranasinghe, V. G. Zakrzewski, J. Gao, N. Rega, G. Zheng, W. Liang, M. Hada, M. Ehara, K. Toyota, R. Fukuda, J. Hasegawa, M. Ishida, T. Nakajima, Y. Honda, O. Kitao, H. Nakai, T. Vreven, K. Throssell, J. A. Jr, J. E. Peralta, F. Ogliaro, M. J. Bearpark, J. J. Heyd, E. N. Brothers, K. N. Kudin, V. N. Staroverov, T. A. Keith, R. Kobayashi, J. Normand, K. Raghavachari, A. P. Rendell, J. C. Burant, S. S. Iyengar, J. Tomasi, M. Cossi, J. M. Millam, M. Klene, C. Adamo, R. Cammi,

J. W. Ochterski, R. L. Martin, K. Morokuma, O. Farkas, J. B. Foresman, and D. J. Fox, *Gaussian 16, Revision A.03*, Gaussian Inc., Wallingford CT, 2016.

20 A. Ghatak and S. Lokanathan, in *Quantum Mechanics: Theory and Applications*, Springer Netherlands, Dordrecht, 2004, pp. 716–741, DOI: **10.1007/978-1-4020-2130-5_26**.

21 Z. Shuai, *Chin. J. Chem.*, 2020, **38**, 1223–1232.

22 D. McCumber, *Phys. Rev.*, 1964, **136**, A954.

23 Q. Peng, Y. Yi, Z. Shuai and J. Shao, *J. Chem. Phys.*, 2007, **126**, 114302.

24 Y. Niu, Q. Peng and Z. Shuai, *Sci. China, Ser. B: Chem.*, 2008, **51**, 1153–1158.

25 Y. Niu, W. Li, Q. Peng, H. Geng, Y. Yi, L. Wang, G. Nan, D. Wang and Z. Shuai, *Mol. Phys.*, 2018, **116**, 1078–1090.

26 Q. Peng, Y. Yi, Z. Shuai and J. Shao, *J. Am. Chem. Soc.*, 2007, 9333–9339.

27 H. Y. Sun, Z. Y. Yu, A. P. Zhou, S. L. Wei, Q. Chang, T. Zhang and Y. P. Sun, *Mol. Phys.*, 2023, **121**, e2156404.